# Surface:Volume Relationship in Cardiac Myocytes Studied with Confocal Microscopy and Membrane Capacitance Measurements: Species-Dependence and Developmental Effects

Hiroshi Satoh, Leanne M. D. Delbridge, Lothar A. Blatter, and Donald M. Bers
Department of Physiology, Loyola University Chicago, Maywood, Illinois 60153 USA

ABSTRACT The quantitative analysis of the contribution of ion fluxes through membrane channels to changes of intracellular ion concentrations would benefit from the exact knowledge of the cell volume. It would allow direct correlation of ionic current measurements with simultaneous measurements of ion concentrations in individual cells. Because of various limitations of conventional light microscopy a simple method for accurate cell volume determination is lacking. We have combined the optical sectioning capabilities of fluorescence laser scanning confocal microscopy and the whole-cell patch-clamp technique to study the correlation between cell volume and membrane capacitance. Single cardiac myocytes loaded with the fluorescent dye calcein were optically sectioned to produce a series of confocal images. The volume of cardiac myocytes of three different mammalian species was determined by three-dimensional volume rendering of the confocal images. The calculated cell volumes were 30.4 ± 7.3 pl (mean ± SD) in rabbits ($n$ = 28), 30.9 ± 9.0 pl in ferrets ($n$ = 23), and 34.4 ± 7.0 pl in rats ($n$ = 21), respectively. There was a positive linear correlation between membrane capacitance and cell volume in each animal species. The capacitance-volume ratios were significantly different among species (4.58 ± 0.45 pF/pl in rabbit, 5.39 ± 0.57 pF/pl in ferret, and 8.44 ± 1.35 pF/pl in rat). Furthermore, the capacitance-volume ratio was dependent on the developmental stage (8.88 ± 1.14 pF/pl in 6-month-old rats versus 6.76 ± 0.62 pF/pl in 3-month-old rats). The data suggest that the ratio of surface area:volume of cardiac myocytes undergoes significant developmental changes and differs among mammalian species. We further established that the easily measurable parameters of cell membrane capacitance or the product of cell length and width provide reliable but species-dependent estimates for the volume of individual cells.

## INTRODUCTION

In virtually every cell type ionic currents across cellular membranes determine the membrane potential and intracellular ion concentrations. In cardiac cells ionic currents constitute the elementary cellular event of excitation-contraction coupling. In many electrophysiological studies the amplitude or the integral of ionic currents has been used to estimate ionic fluxes through ion channels and was studied comparatively among different animal species (Wang et al., 1993; Wettwer et al., 1993), different developmental stages (Huynh et al., 1992), and various pathological states such as cardiac hypertrophy (Scamps et al., 1990; Tomita et al., 1994) and cardiomyopathy (Keung et al., 1991; Rossner, 1991). For example, the cytosolic calcium buffering properties have been estimated from integration of voltage-dependent transsarcolemmal calcium currents in rat cardiac myocytes (Berlin et al., 1994) and chromaffin cells (Neher and Augustine, 1992).

The amplitude of the ionic currents is dependent not only on membrane potential and transsarcolemmal ionic gradients but also on cell size. For comparative purposes, membrane currents and membrane conductance in general are often normalized to the cell membrane capacitance, thereby expressing ion movements through channels as current densities (e.g., pA/pF). This approach takes advantage of the fact that the "specific capacitance" of cell membranes is approximately 1 $\mu$F/cm$^2$ and is fairly constant among different muscle cell types and species (Hille, 1992). Therefore, cell capacitance measurements by electrophysiological methods are widely used to estimate the surface membrane area of cells and as an indirect index of cell volume.

Because it is ultimately the critical change of the concentrations of intracellular ions (e.g., calcium and protons) produced by ionic currents that trigger and control cellular events such as contraction, exocytosis, and cell proliferation, it would be desirable to relate ionic currents directly to cell volume. Unfortunately the surface membrane area that can be estimated easily by membrane capacitance measurements is only of limited use as an estimator of cell volume because the degree of membrane folding and the abundance of membrane invaginations are highly variable among different cell types and animal species (Page, 1978; Bers, 1991) and depend on the developmental stage (Page et al., 1974; Delcarpio et al., 1989). Furthermore, routine accurate measurements of cell volume in intact living cells are not trivial because of the lack of sufficient axial resolution of conventional light microscopes. Thus it would be particularly useful to know what the surface area:volume ratio is for given cell types.

Laser scanning confocal microscopy (LSCM) technique offers considerably improved spatial resolution over conventional light microscopy and overcomes certain limitations (Blatter and Wier, 1992) of standard video fluorescence microscopy in imaging intact cells. LSCM allows

*Received for publication 24 July 1995 and in final form 28 November 1995.*
Address reprint requests to Dr. Lothar A. Blatter, Department of Physiology, Loyola University Chicago, 2160 South First Avenue, Maywood, IL 60153. Tel.: 708-216-6305; Fax: 708-216-6308; E-mail: lblatte@luccpua.it.luc.edu.

0006-3495/96/03/1494/11 $2.00

detection of fluorescence signals with high spatial and temporal resolution from uniformly thin optical sections at variable cell depths (Wright et al., 1993). Optical cell sections obtained with LSCM have been used for three-dimensional (3D) reconstructions of subcellular structures (Stevens, 1994) and for the quantitative analysis of cell volume of various cell types such as human Langerhans' cell (Scheynius et al., 1992), rat renal collecting duct cell (Tinel et al., 1994), rat hippocampal pyramidal cell (Cohen et al., 1994), rat lung Clara cell (Dodge et al., 1994), and rabbit cardiomyocyte (Chacon et al., 1994).

The goals of the present study were threefold: first, using LSCM, to attempt to accurately measure cell volume of cardiac myocytes from several mammalian species at different developmental stages of the animals; second, to establish simple relationships between cell volume and surface membrane area as measured with the whole-cell patch-clamp technique and expressed as cell capacitance (pF/pl); and third, for the benefit of other investigators, to correlate cell volume with parameters, such as cell length and cell width, that can be measured easily by conventional light microscopy without having to use confocal microscopy.

We compared cell volume-capacitance relationships in rabbit, ferret, and rat ventricular myocytes. In rat myocytes we examined further the changes of this relationship that occurred during development. Our results showed linear correlations between membrane capacitance and cell volume in all experimental groups. These relationships varied among different animal species and different developmental stages, indicating significant differences in membrane folding or density of transverse tubules.

## MATERIALS AND METHODS

### Experimental groups

The following experimental groups were used. For the comparison of cell volume and cell membrane capacitance among different species adult New Zealand White rabbits (2.3–2.8 kg), adult male ferrets (1–1.3 kg), and adult male Sprague-Dawley rats (415–516 g) were used. To investigate the influence of developmental stage 3-month-old adolescent rats (330–378 g) were compared with a subpopulation of adult rats that were 6 months old (480–516 g).

### Cell isolation

Ventricular myocytes were isolated by an enzymatic procedure as described previously (Hryshko et al., 1989). Briefly, the animals were anesthetized by intravenous (rabbits, 50–75 mg/kg) or intraperitoneal (ferrets, 100 mg/kg; rats, 180 mg/kg) injection of sodium pentobarbital. The hearts were excised, flushed with nominally $Ca^{2+}$-free Tyrode solution, and perfused using a Langendorff perfusion apparatus. Initially, hearts were perfused with nominally $Ca^{2+}$-free Tyrode solution (5 min) followed by 0.8–0.95 mg/ml collagenase (Type B; Boehringer Mannheim) and 0.1 mg/ml pronase (Boehringer Mannheim) for 15–25 min. After sufficient enzymatic digestion the tissue was mechanically dispersed, filtered, and repeatedly rinsed while gradually increasing extracellular calcium ($[Ca^{2+}]_o$). The cells were then plated in the experimental superfusion chamber (~0.5 ml). The glass coverslip that formed the bottom of the chamber was pretreated with laminin (Collaborative Research, Bedford, MA) to enhance cell adhesion. Cells were superfused with a modified Tyrode solution containing (in mM) 140 NaCl, 6 KCl, 1 $MgCl_2$, 5 HEPES, 10 glucose, and 2 $CaCl_2$ (1 $CaCl_2$ for rat). pH was adjusted to 7.4 with NaOH. Experiments were carried out at 23°C.

### Measurements of membrane capacitance

Whole-cell voltage-clamp experiments were conducted using patch electrodes fabricated from 1.5-mm borosilicate capillary tubing (World Precision Instruments, Sarasota, FL). Pipettes contained (in mM) 125 CsCl, 10 MgATP, 20 HEPES, 0.3 GTP, and 10 ethylene glycol-bis($\beta$-aminoethyl ether) *N,N,N′,N′*-tetraacetic acid (EGTA); pH was adjusted to 7.4 with CsOH. With this filling solution the pipette resistance typically was 1–2 MΩ. An Axopatch 200A patch-clamp amplifier (Axon Instruments, Foster City, CA) was used for membrane potential control and current recordings. Voltage protocol generation, data acquisition, storage, and analysis were performed with the software package pCLAMP (version 6.0.1.; Axon Instruments).

After rupturing the cell membrane and establishing whole-cell configuration the cell capacitance was measured. The membrane capacitance was calculated from 5-mV hyperpolarizing and depolarizing steps (20 ms) applied from a holding potential of −80 mV according to the equation (Benitah et al., 1993)

$$C_M = \tau/\Delta V_M * I_0/(1 - I_\infty/I_0),$$

where $C_M$ is membrane capacitance, $\tau$ is the time constant of the capacitance current relaxation, $I_0$ is the peak capacitive current determined by single exponential fit and extrapolation to the first sample point after the voltage step $\Delta V_M$, and $I_\infty$ is the amplitude of steady-state current during the voltage step. This method of cell membrane capacitance measurement has the advantage over procedures that depend on integration of membrane currents in that it is independent of the sampling duration and would account for the presence of any finite membrane conductance during the voltage step. Capacitive currents were sampled at 20 kHz and filtered at 5 kHz. The capacitive currents were independent of the polarity of the voltage steps in individual cells, and no sodium currents were activated during depolarizing steps.

### Cell volume measurements with laser scanning confocal microscopy

#### *General approach*

The general approach chosen for the quantitative determination of cell volume involved the acquisition of a stack of images of cellular fluorescence obtained at high spatial resolution throughout the entire depth of the cell. After adequate processing (see below) the stack of images was used to reconstruct (render) the cell volume in three dimensions.

To label the intracellular space, myocytes were loaded with the fluorescent indicator calcein. Calcein is evenly distributed throughout the cell, is largely unaffected by changes in the intracellular environment, is not contaminated by cellular autofluorescence, and has been used previously for volume measurements (e.g., Guilak, 1994; Chacon et al., 1994). Dye loading was achieved by exposure of myocytes to the membrane-permeant calcein/acetoxymethyl (AM) ester (5 $\mu$M; Molecular Probes, Eugene, OR) for 30 min at room temperature. Excess extracellular dye was removed by exchanging the bathing medium three times. An additional 30 min was allowed for intracellular hydrolysis of calcein/AM before capacitance and volume measurements were performed.

#### *Laser scanning confocal microscopy*

Calcein fluorescence imaging was performed on a laser scanning confocal microscope (LSM 410; Carl Zeiss, Oberkochen, Germany) equipped with an argon ion laser (model 2014 series, 25 mW; Uniphase, San Jose, CA)

and coupled to an inverted microscope (Axiovert 100; Carl Zeiss). The objective lens was a Zeiss 40× oil immersion Plan-Neofluar with a numerical aperture of 1.3. Calcein fluorescence was excited with the 488-nm line of the argon laser. The laser power was kept at the lowest level and the excitation light intensity was further attenuated by 90% with a neutral density filter (ND = 1.0) in the excitation path to minimize photobleaching and phototoxicity. The laser excitation beam was directed to the specimen through a 510-nm dichroic beam splitter. Emitted fluorescence was collected through a 515-nm long-pass emission filter in front of a photomultiplier tube.

For the acquisition of a stack of images the objective was moved in the axial direction ($z$ dimension) with a stepping motor under computer control. Depending on the thickness of individual myocytes, 20–35 sections at 1.2-$\mu$m steps were obtained. At each optical plane the cell was scanned once to produce a cell fluorescence image ($x$, $y$ scan) of 512 by 512 pixels. Magnification was set by the objective and the zoom factor of the LSCM to give a pixel size of approximately 0.1 $\mu m^2$ (~0.3 $\mu$m * ~0.3 $\mu$m). This magnification allowed imaging of the entire myocyte at a spatial resolution near the theoretical $x$, $y$ resolution of the system (numerical aperture = 1.3). The duration of an entire $x$, $y$ scan was 1.04 s, exposing an individual pixel to the laser light for <4 $\mu$s. The analog output of the photomultiplier tube was digitized at 8-bit resolution representing fluorescence intensities with 256 levels of grey.

### *Thresholding and background subtraction*

For quantitatively accurate cell volume determination, correct discrimination of cellular fluorescence intensities (thus representing cell volume elements) from background fluorescence, image noise, and out-of-focus fluorescence is crucial. Several steps were undertaken to eliminate noncellular volume elements (voxels) from the volume calculations. In each experiment offset and gain of the system were chosen to represent noncellular background near zero and fluorescence intensities from cellular elements to cover the full range of 256 intensity levels without saturation of the recording system. With this approach the need for additional background subtraction procedures was eliminated. Photobleaching was kept to a minimum, as discussed below. Because the spatial resolution in the axial direction ($z$ dimension) was estimated to be <1 $\mu$m in our system, out-of-focus contributions from adjacent sections were minimized by choosing a sectioning interval of 1.2 $\mu$m. Because of the limits of spatial resolution of the system and the finite size of the sampled volume elements, voxels at the cell border only partially represent cellular volumes. On the level of an individual voxel this results in a variable decrease of fluorescence intensity, depending on the degree by which an individual voxel is filled by cell volume.

Elimination of out-of-focus fluorescence and noncellular contributions from voxels at the cell border were achieved by photometric thresholding of the fluorescence images. The level of thresholding was determined empirically. Fig. 1 *A* shows a frequency histogram of fluorescence intensities of a central section of a cardiac myocyte. The frequency histogram shows a clear peak around a fluorescence intensity value of about 150 that could be fitted perfectly by a simple gaussian distribution (*dashed line*). This peak represents the distribution of wholly cellular pixels. To account for extracellular pixels and "partial" cellular pixels the gaussian fit was subtracted from the measured frequency distribution (Fig. 1 *B*). The frequency distribution after subtraction did not reveal any specific peaks ($n$ = 10 cells analyzed), except a small peak near intensity zero representing noncellular background. From the lack of peaks in the remaining distribution of intensities we concluded that pixels with random fractional cell volume between 0 and 1 account for most of the residual area in Fig. 1 *B*. We therefore attributed a weighing factor of 0.5 to these pixels. Because this area is half of the box in Fig. 1 *B*, this would also correspond to an effective threshold level of 50 for the stack of fluorescence images obtained at different axial planes. The critical dependence of the volume calculation on the photometric threshold level on the volume calculation is shown in Fig. 1 C ($n$ = 8 cells analyzed).

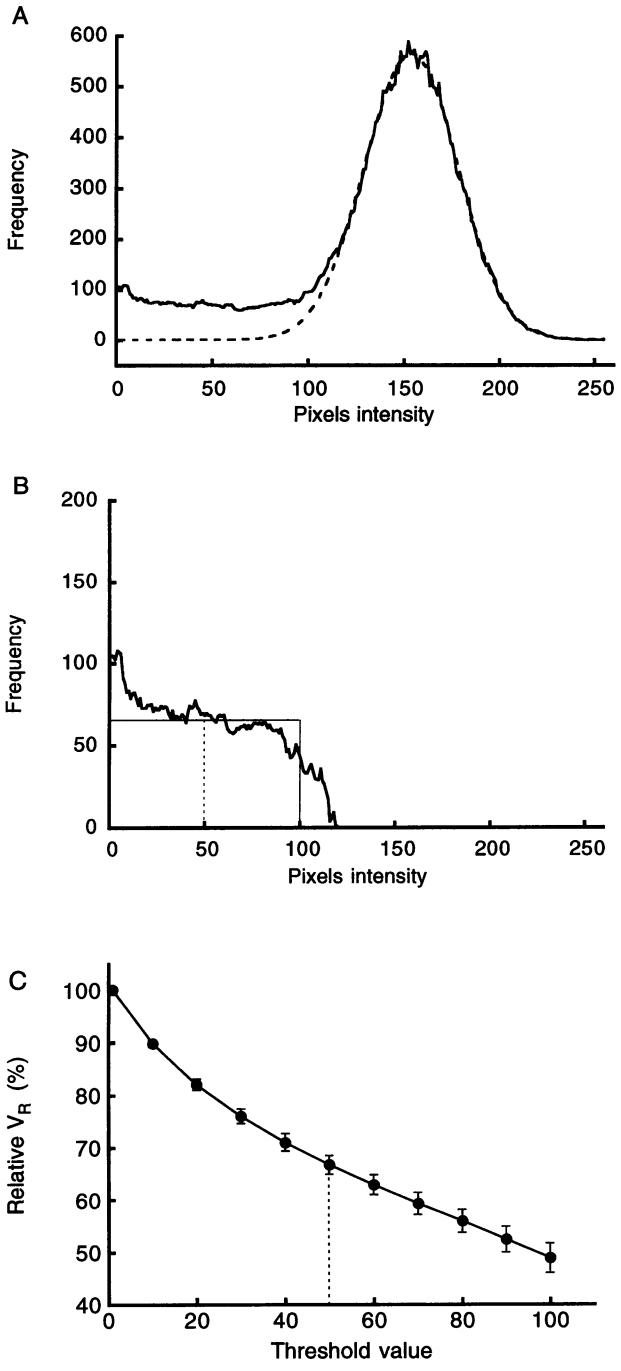


FIGURE 1 (*A*) Frequency distribution of pixel intensities from a central section through a calcein-loaded rabbit ventricular myocyte. The dashed line represents a gaussian fit to the frequency peak centered around a pixel intensity of 150. (*B*) Difference distribution of pixel intensities obtained by subtraction of the gaussian fit from the frequency histogram in *A*. From the difference frequency distribution a thresholding value of 50 was derived (for details see text). (*C*) Effect of level of thresholding on estimates of rendered cell volume. The data from eight cells were normalized to the volume value measured with no thresholding.

### *Photobleaching of calcein fluorescence*

Because thresholding was applied to the confocal images it was necessary to estimate the degree of photobleaching encountered during data acqui-

sition to avoid the elimination of volume information that would fall below the set threshold because of photobleaching. Care was taken to keep photobleaching to a minimum by choosing the lowest laser power and by attenuation of the excitation intensity by neutral density filters. Photobleaching of intracellular calcein was estimated by repetitively scanning cardiac myocytes at the same focal plane (1-s scan intervals). The residual fluorescent intensity after 30 consecutive scans was 86.8 ± 8.1% of the initial value ($n$ = 10 cells). Although photobleaching occurred in our experiments its degree was considered negligible because of the sufficient signal-to-noise ratio (see Fig. 1 *A*). Furthermore, the focal plane was moved in the axial direction between individual scans, thereby reducing the degree of bleaching within an individual plane. Therefore, no correction for photobleaching was applied.

### *Accuracy of axial spacing of optical sections*

Quantitative volume rendering based on optical sections obtained at variable axial depth is critically dependent on accurate movement of the objective in the axial direction ($z$ dimension). We performed independent measurements of the axial travel of the stepping motor that moves the objective of the LSM 410. By moving an object in the vertical direction with a piezoelectrical device (micromanipulator model PCS-1000-H; Burleigh Instruments, Fishers, NY), the travel distance of the manipulator was compared with the nominal travel of the stepping motor or objective, respectively. An object (a tip of glass pipette) was displaced by variable distances between 0 and 70 μm in the $z$ direction by the micromanipulator. The object was then refocused and the nominal movement of the stepping motor was correlated with the $z$ travel of the manipulator. Over the whole distance tested (70 μm) the $z$ displacement of the microscope stepping motor and piezoelectric manipulator showed a high linear correlation, with a slope of 1.05 ($r^2$ = 0.99, $p < 0.01$; $n$ = 10 trials). These data indicated that the $z$ movements of the objective were correctly calibrated and therefore the spatial separation of successive optical sections was uniform.

### *Refractive index mismatch and spherical aberration: volume correction factor*

Mismatch of refractive indices of specimen, mounting medium, and lens immersion medium causes spherical aberration and distortion of morphological data. We have investigated the degree of spherical aberration in our experiments by optically sectioning objects of known geometry and dimensions, and with fluorescent properties similar to calcein-loaded myocytes. Fluorescent latex beads of 2.0 and 15.5 μm diameter were chosen (exact diameters measured by electron microscopy; Molecular Probes) that had fluorescence properties very similar to those of calcein (excitation 488 nm; emission >515 nm). The $x$, $z$ reconstruction of a 2-μm bead that appeared perfectly spherical in the $x$, $y$ plane (Fig. 2 *Aa*) shows deformation into an elongated oval in the $z$ dimension (see Fig. 2 *Ab*). This distortion, which results from spherical aberration, becomes more pronounced at increasing depth into the specimen (Fig. 2 *Ac*). Distortion through spherical aberration is particularly accentuated at the boundary of fluorescent and nonfluorescent objects of different refractive index (e.g., cell border). Furthermore, mismatch of refractive index of lens immersion medium (oil) and mounting medium (water) has the consequence that the movement of the focal plane in a specimen does not necessarily follow the movement of the objective when acquiring optical $z$ sections through an object. If the refractive index of the immersion medium (in our study an oil immersion objective was used; refractive index $r_{oil}$ = 1.48) is larger than the refractive index of the specimen and its mounting medium (in our case the cellular environment was approximated by the refractive index for water: $r_{water}$ = 1.33) then the distance traveled by the plane of focus is smaller than the nominal $z$ movement of the objective. As a consequence the $z$ extension of the specimen and therefore the reconstructed volume would be overestimated. Even with confocal microscopy with its significant higher spatial resolution, uncompensated spherical aberration can generate errors up to 50% (Majlof and Forsgren, 1993) in quantitative measurements that include the depth dimension.

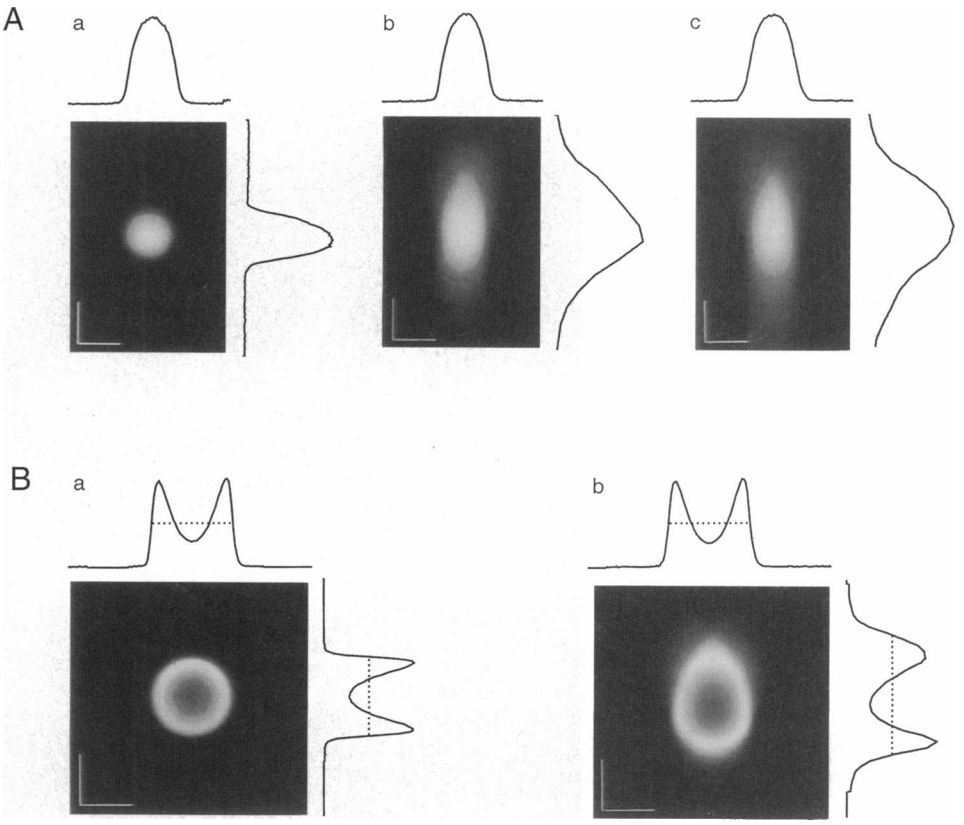


FIGURE 2 Confocal imaging of fluorescent microspheres. (*A*) Microspheres of 2.0 μm diameter were sectioned by recording $x$, $y$ scans at 0.8-μm axial steps. Calibration bar = 2 μm. (*a*) $x$, $y$ image and corresponding normalized intensity profiles across the center of the bead; $x$, $z$ reconstruction of the same bead directly on the coverslip (*b*) and 22 μm above the objective lens (*c*). (*B*) $x$, $y$ and $x$, $z$ images of a fluorescent bead of 15.5 μm diameter, including normalized $x$, $y$, and $z$ fluorescence profiles recorded from the center region of the bead. The donut-shaped appearance of the bead image is due to the lack of fluorophores in the center of the microsphere. The dashed lines indicate the full width at half-maximum fluorescence intensity. Calibration bar = 10 μm. Images were recorded with a Zeiss 40× oil immersion Plan-Neofluar objective with a numerical aperture of 1.3. Refractive index of immersion oil = 1.48.

For our volume measurements of cardiac myocytes we have chosen an empirical method to compensate for such distortions. This method is based on the volume reconstruction of known objects with the confocal sectioning technique. Optical sections of fluorescent spherical latex beads with a diameter similar to the thickness of a cardiac myocyte (bead diameter = 15.5 $\mu$m) were obtained at regular $z$ intervals with the LSM 410. Fig. 2 *Ba* shows an $x$, $y$ image of a fluorescent sphere, revealing its perfectly circular cross section. Fig. 2 *Bb* shows an $x$, $z$ reconstruction of the same bead, revealing a substantial elongation of the object in axial direction. The normalized intensity profiles through the center of the microsphere and the full width at half-maximum diameter (FWHM, dashed line in the normalized intensity profiles) of the sphere were identical in the $x$ and $y$ dimensions, indicating lack of distortion within the focal plane. The FWHM in the $z$ dimension was approximately 1.46 times larger than the FWHM in the $x$ and $y$ dimensions, respectively (Fig. 2 *Bb*, *dashed lines*). We calculated a volume correction factor based on the 3D reconstruction of beads. The apparent volume of the bead as reconstructed from the optical sections was calculated by approximating the geometry of the imaged sphere as an ellipsoid with a diameter of the FWHM in the $x$ dimension and a height corresponding to the FWHM in the $z$ dimension. A correction factor was calculated from dividing the true spherical volume by the apparent ellipsoidal volume. This correction factor ($V_{sphere}/V_{ellipsoid} = 0.68$) was applied to the estimated cell volumes of cardiac cells (see below).

### *Cell volume measurements from two-dimensional optical sections: three-dimensional volume-rendering algorithm*

For the cell volume measurements a stack of 20–35 calcein fluorescence images, depending on the thickness of the cell, were obtained at optical planes 1.2 $\mu$m apart (Fig. 3 *A*). The images were analyzed with the Zeiss LSM software (version 3.70). The surface area of each section was determined by multiplying the number of cellular pixels above the chosen threshold value (e.g., 50 in Fig. 1, *B* and *C*) with the size of an individual pixel (given by the magnification factor of objective and the zoom factor of the LSCM). The raw value for the cell volume (picoliters or cubic microns) was calculated by multiplying the number of all significant pixels from all sections with the $z$ interval of individual sections (1.2 $\mu$m). The raw volume values were then scaled by the volume correction factor of 0.68 to account for volume distortions due to spherical aberration. Fig. 3 *B* shows a 3D volume representation of a cardiac myocyte. The cell was reconstructed by describing its three-dimensional surface contour as a set of polygons. The method used was similar to the marching cube algorithm described by Lorensen and Cline (1987). Volume rendering and surface topography reconstruction were performed using the programming language IDL (Interactive Data Language; Research Systems, Boulder, CO).

## Experimental protocol

Volume measurement and cell membrane capacitance were obtained for each cardiac myocyte. After dye loading and washing, optical sectioning was performed. After recording of the images whole-cell voltage-clamp configuration was established and the membrane capacitance was measured as described. Routinely, optical sectioning was performed before the voltage clamp experiments because the mechanical movement of the focal plane would interfere with forming and maintaining a gigaseal connection with the microelectrode. Therefore, intracellular perfusion with a calcium buffer (EGTA) during membrane capacitance measurements could potentially lead to changes in cell volume due to relaxation. In our experiments such volume changes were absent or were negligible (see Discussion).

## Statistical analysis

Results are expressed as means ± SD for the indicated number ($n$) of myocytes. Student's $t$-test and one-way analysis of variance (ANOVA) were used for statistical analyses, and the probability was considered significant at $p < 0.05$. Correlation was calculated by Pearson's linear correlation coefficient.

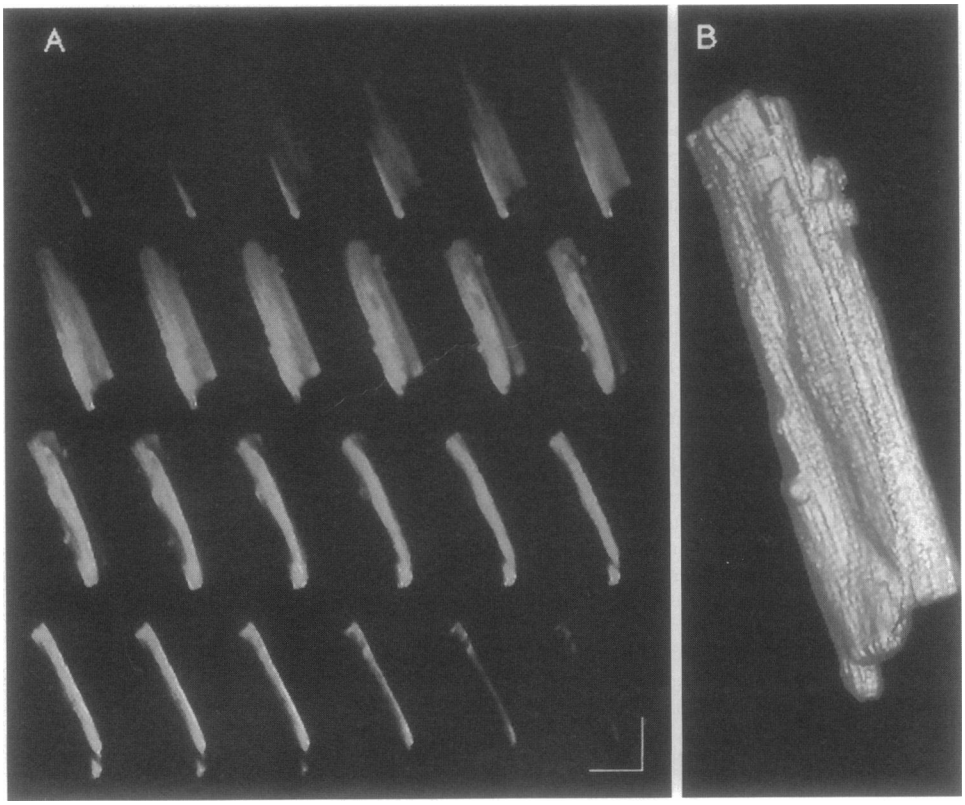


FIGURE 3 (*A*) Serial confocal optical sections recorded from a representative rat ventricular myocyte, loaded with the fluorescent dye calcein. Twenty-four optical sections were taken at 1.2 $\mu$m axial intervals. Calibration bar = 50 $\mu$m. Individual images are oriented from the bottom to the top (*upper left corner*, top section; *lower right corner*, bottom section). (*B*) Three-dimensional reconstruction of a cardiac myocytes from optical sections shown in *A*.

## RESULTS

### Cell dimensions and volume measurements in mammalian cardiac myocytes

With the use of the optical sectioning capabilities of a confocal microscope and volume-rendering techniques, we reconstructed the three-dimensional geometry of single cardiac myocytes, and we determined the cell volume in three different mammalian species. Fig. 3 *B* illustrates the irregular and complex surface topography of single cardiac cells, including branches, dents, membrane invaginations, and transverse tubules. The average values for the cell volumes were 30.4, 30.9, and 34.4 pl, respectively, in adult rabbits, ferrets, and rats (Table 1). There were no differences in average maximal cell length and width among different species. Rabbit myocytes, however, showed a small but significant difference in cell thickness ($z$ dimension) as compared to rat and ferret myocytes.

Volume rendering based on optical sectioning (Fig. 3) requires special equipment and relies on computational image-processing routines that are not always suitable or applicable to experimental studies in which knowledge of the cell volume would be essential. We therefore aimed to provide a simple morphological measurement that could serve as a reliable estimate of cell volume in cardiac cells. Fig. 4 *A* shows the rendered cell volume ($V_R$), measured by optical sectioning, as a function of the simple product of maximum cell length and width (easily measured in nonconfocal microscopy). There was significant linear correlation between cross-sectional cell area and rendered cell volume for all species. This result indicates that cell length and width are useful parameters for extrapolating cell volume with conventional light microscopy. From the regression line in Fig. 4 *A*, $V_R$ (picoliters) can be expressed as $6.59 * 10^{-3}$ pl/$\mu m^2$ * cell area ($\mu m^2$) in rabbits, as $7.21 * 10^{-3}$ pl/$\mu m^2$ * cell area ($\mu m^2$) in ferrets, and as $7.59 * 10^{-3}$ pl/$\mu m^2$ * cell area ($\mu m^2$) in rats, respectively.

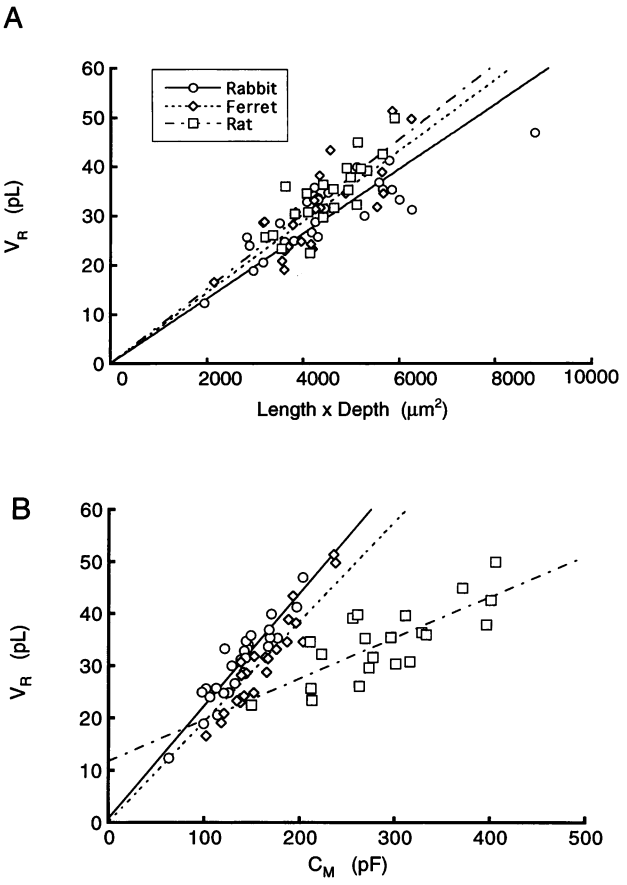


FIGURE 4. (*A*) Correlation between cross-sectional area and rendered cell volume in three different mammalian species. Cross-sectional area was calculated as the product of maximal cell length and width. (*B*) The relationship between membrane capacitance ($C_M$) and rendered cell volume ($V_R$) in rabbit ($n$ = 28), ferret ($n$ = 23), and adult rat ($n$ = 21) ventricular myocytes. There was a significant linear correlation between membrane capacitance and cell volume in each animal. The regression lines were $V_R = 0.215 * C_M + 0.718$, $r^2 = 0.86$ ($p < 0.01$) in rabbits, $V_R = 0.192 * C_M + 0.070$, $r^2 = 0.86$ ($p < 0.01$) in ferrets, and $V_R = 0.078 * C_M + 11.755$, $r^2 = 0.58$ ($p < 0.01$) in rats, respectively.

### Relationship between cell volume and membrane capacitance

In whole-cell voltage-clamp studies measurement of the cell membrane capacitance is routinely carried out using a simple voltage-clamp protocol (see Materials and Methods). Cell membrane capacitance was measured for the same cells that had undergone volumetric analysis. The average membrane capacitance was 138 pF in rabbits, 162 pF in ferrets, and 289 pF in adult rats (Table 1). The average membrane capacitance was significantly higher in rats, whereas rabbit myocytes did not differ significantly from ferret myocytes (Table 1).

**TABLE 1 Morphometric data in rabbit, ferret, and rat ventricular myocytes**

| | Rabbit (5) | Ferret (7) | Rat (6) |
|---|---|---|---|
| Cells ($n$) | 28 | 23 | 21 |
| Length ($\mu m$) | 142.8 ± 29.5 | 138.0 ± 22.7 | 141.9 ± 14.9 |
| Width ($\mu m$) | 31.9 ± 9.5 | 31.0 ± 5.3 | 32.0 ± 4.8 |
| Depth ($\mu m$) | 12.2 ± 1.7 | 14.0 ± 2.8* | 13.3 ± 1.6* |
| $V_R$ (pl) | 30.4 ± 7.3 | 30.9 ± 9.0 | 34.4 ± 7.0 |
| $C_M$ (pF) | 138.0 ± 31.3 | 162.4 ± 35.6 | 289.2 ± 68.8*‡ |
| $C_M/V_R$ (pF/pl) | 4.58 ± 0.45 | 5.39 ± 0.57* | 8.44 ± 1.35*‡ |

$V_R$, rendered cell volume; $C_M$, membrane capacitance. Values are means ± SD. Number of hearts from each species in parenthesis.
*$p < 0.01$ vs. rabbit.
‡$p < 0.01$ vs. ferret.

We tested the hypothesis that the membrane capacitance could provide a useful estimate for the cell volume of individual cells. Fig. 4 *B* shows the correlation between membrane capacitance and cell volume (*C-V* relationship) for the three mammalian species. The membrane capacitance ($C_M$) correlated linearly with the rendered cell volume ($V_R$); however, the regression lines were different among animal species and the variability of the data was larger in rats (correlation coefficient $r^2 = 0.58$) than in rabbits ($r^2 = 0.86$) and ferrets ($r^2 = 0.86$). Despite the large variability of

cell sizes (range: 12–51 pl) the *C-V* relationship was highly constant in rabbits and ferrets and to a lesser degree in rats. Although constant within individual species, the *C-V* relationship was different for rabbit, ferret, and rat myocytes.

The species differences of the *C-V* relationship were further analyzed by calculating the ratio of capacitance to rendered volume ($C_M/V_R$) for individual cells. These values are plotted in Fig. 5 for the three different species. The mean values for $C_M/V_R$ were 4.58 ± 0.45 pF/pl in rabbits, 5.39 ± 0.57 pF/pl in ferrets, and 8.44 ± 1.35 pF/pl in rats. The average value measured in rats was significantly higher than the values measured in ferrets and rabbits. The $C_M/V_R$ ratio of ferrets and rabbits differed by only about 15%; however, the difference was statistically significant ($p < 0.01$ by ANOVA).

### Developmental dependence of the capacitance-volume relationship in rats

Although it has been shown that aging affects both cell membrane capacitance (Huynh et al., 1992) and cell volume (Fraticelli et al., 1989), there are no studies on the relationship between these two parameters. We therefore directly compared the *C-V* relationship of cardiac myocytes from adolescent (3-month-old) and adult (6-month-old) rats. Table 2 summarizes the body weight, cell dimensions, cell volume, and membrane capacitance of these two experimental groups. Both $V_R$ and $C_M$ increased with age. It was primarily an increase in cell length at the later developmental stage that accounted for the increase in cell volume. In Fig. 6 the ratio $C_M/V_R$ of adolescent and adult rats is compared. The average $C_M/V_R$ ratio of 8.88 ± 1.14 pF/pl in adult rat was significantly higher than in adolescent rats (6.76 ± 0.62 pF/pl; $p < 0.01$).

**TABLE 2 Morphometric data in adolescent and adult rat myocytes**

| | Adolescent (4) | Adult (4) |
|---|---|---|
| Body weight (g) | 346 ± 22 | 496 ± 15** |
| Cells (*n*) | 14 | 14 |
| Length (μm) | 123.8 ± 14.4 | 140.1 ± 16.4** |
| Width (μm) | 33.6 ± 6.7 | 33.4 ± 4.8 |
| Depth (μm) | 12.8 ± 1.4 | 13.8 ± 1.5 |
| $V_R$ (pl) | 30.9 ± 5.2 | 36.8 ± 6.3* |
| $C_M$ (pF) | 207.2 ± 30.5 | 323.9 ± 51.8** |
| $C_M/V_R$ (pF/pl) | 6.76 ± 0.62 | 8.88 ± 1.14** |

Values are means ± SD. Adolescent, myocytes from 3-month-old animals; Adult, 6-month-old animals. Number of hearts in parenthesis.
*$p < 0.05$ vs. adolescent rat myocytes.
**$p < 0.01$ vs. adolescent rat myocytes.

## DISCUSSION

### Volume rendering based on optical sectioning with laser scanning confocal microscopy

The availability of laser scanning confocal microscopes, suitable fluorescent probes, and advanced computational image processing routines has enabled morphometric studies of intact living cells at significantly higher spatial resolution and with much improved fidelity. Nevertheless, these methods can be subject to various sorts of artifacts that preclude accurate quantitative measurements. Distortions may arise from motion artifacts occurring during data acquisition, from inaccuracies of background subtraction and thresholding, and from erroneous estimation of axial distances due to the optical limitations of spatial resolution, which are the result of spherical aberration and other problems related to optical sectioning of thick specimens.

Because volume measurements were performed on intact cardiac cells that maintained their potential to contract, but were quiescent, care was taken to avoid motion artifacts (i.e., spontaneously contracting cells were excluded). Furthermore, the adherence of the cells to the bottom of the

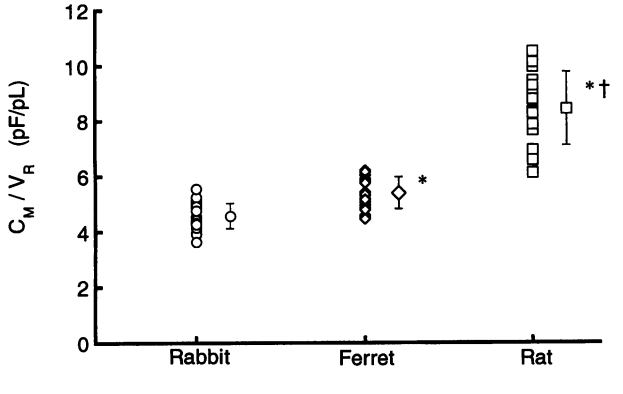


FIGURE 5 Plots of the ratio of membrane capacitance to cell volume ($C_M/V_R$: pF/pl) in individual rabbit, ferret, and adult rat myocytes. The larger symbols to the right in each column represent mean values ± SD. Statistical analysis (ANOVA): * $p < 0.01$ versus rabbit; † $p < 0.01$ versus ferret.

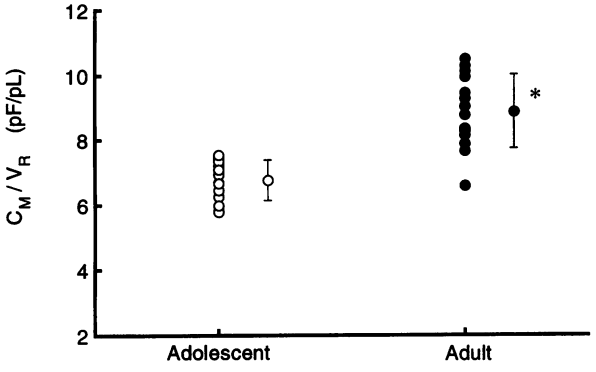


FIGURE 6 Effect of developmental stage on the capacitance-volume ratio ($C_M/V_R$: pF/pl). The $C_M/V_R$ ratio in adult rat cells was significantly higher than in adolescent cells (* $p < 0.01$). The larger symbols show means ± SD.

experimental chamber was enhanced by pretreating the coverslips with laminin.

The choice of the correct photometric threshold crucially affects the calculated cell volume (see Fig. 1 *C*). We have set threshold levels based on the analysis of the frequency distribution of the intensities of image elements (pixels) recorded from calcein-loaded myocytes. This analysis allowed distinction and compensation for noncellular background near the cell border, volume elements completely filled by cellular elements, and image elements that were only partially filled (but to various degrees) with cell elements. The latter phenomenon occurs at the cell border and is the result of the finite spatial resolution of the image (pixelization). This algorithm is also sensitive to the irregular three-dimensional topography (membrane invaginations, dents, and branches) typical for isolated cardiac myocytes. The approach efficiently eliminates volume elements that in a given section through the cell, particularly near the bottom or the top, would appear within the boundaries of the cell but which, in fact, represent extracellular space.

An important issue relates to factors that affect the accuracy of the measurement of the depth dimension of the cells. Guilak et al. (1994) have shown that a number of 20 or more sections in axial dimension ($z$ dimension) are necessary to achieve an acceptable signal-to-noise ratio (10:1 or better). In our experiments, optical sections were obtained at nominal $z$ steps of 1.2 $\mu$m. This way the number of sections per cell was kept between 20 and 35 in all of our experiments. This value was chosen to keep the degree of unnecessary overlap between optical sections in the $z$ dimension at a minimum (because the spatial resolution of the LSCM in the $z$ dimension is only slightly smaller than 1 $\mu$m) without losing significant spatial information between sections, to minimize the contribution from out-of-focus fluorescence, and to minimize photobleaching, which is a direct result of the number of applied scans (and therefore exposure time) to the specimen.

Finally, spherical aberration and axial distortion resulting from mismatch of refractive indices of the immersion medium, mounting medium, and the cell can constitute serious problems in any quantitative measurements in light microscopy that involve the depth dimension of the specimen, leading to significant errors in the estimation of the $z$ dimension. We have approached this problem empirically by imaging an object of known dimension (microspheres with known diameter) and fluorescence properties similar to those of calcein. From the known geometrical dimensions and the measured distortions we calculated a volume correction factor that was applied to the raw estimates of cell volume from the optical sections. Although this method has the advantage of applying a correction factor that was obtained empirically on the same instrument under similar experimental conditions, it has its limitations. For example, the cardiac myocytes have a more complex geometry than the microspheres and do not fully account for the fact that the degree of spherical aberration becomes larger as the depth into the specimen increases (Fig. 2, *Ab* and *Ac*).

## Cell volume measurements in cardiac myocytes

The average cell volumes measured in cardiac myocytes from three different mammalian species were similar and ranged from 30.4 pl in rabbits to 34.4 pl in adult rats. The average cell volume for ferrets was 30.9 pl, after volume correction for spherical aberration. There were no significant differences between cell length and cell width among species. Rabbit ventricular myocytes appeared to be slightly but significantly thinner (Table 1).

Our volume measurements also compare well with the range reported in the literature. For rat myocytes volume values between 16 and 45 pl (measured with light scatter flow cytometry and Coulter analysis) have been reported (Nash et al., 1979; Campbell et al., 1987; Vliegen, 1987; Fraticelli et al., 1989). Gerdes et al. (1986) reported a range of 5–25 pl based on morphometric measurements of stained rat tissue. In other species, Smith and Bishop (1985) measured an average cell volume of 36 pl in ferret hearts, and Campbell et al. (1987) reported 29 pl for guinea pigs. Poole-Wilson (1995) reviewed studies on human myocytes that reported values between 15 and 52 pl. In rabbits Drewnowska and Baumgarten (1991) calculated cell volume ranging from 35 to 43 pl based on measurements of cross-sectional area and cell thickness. Finally, Chacon et al. (1994) reported a value of 60 pl for cardiac myocytes measured with an approach similar to ours using fluorescence confocal microscopy. However, in this study the authors did not make any attempt to correct for spherical aberration and used a different thresholding procedure.

We compared our volume measurements with calculated volumes based on the measured cell dimensions and assumed geometries. Assuming a simple geometry of a rectangular parallelepiped (maximum length * width * depth) the rendered volume values are 54% of the volume of the parallelepiped. Our measured average volume was 42% larger than the calculated volume assuming spindle-shaped cell geometry, but was 29% smaller when a rod-shaped geometry with an ellipsoidal cross-section was assumed. These comparisons indicated that our volume estimations were within the appropriate range.

## Membrane capacitance measurements and the relationship between capacitance and cell volume

Despite the similarities in cell volume among the three species investigated there were significant species-dependent differences in membrane capacitance. Because it is well established that the relationship between capacitance and unit cell membrane is fairly constant among species and cell types (approximately 1 $\mu$F/cm$^2$; for reference see Hille, 1992) it must be concluded that there is a significant species-dependent difference in total surface membrane area. In other words, different species show different degrees of membrane folding, membrane invaginations, and, in cardiac cells, possibly number and/or size of transverse tubules

(t-tubules). Interestingly, in all three species the cell membrane capacitance was linearly correlated with the cell volume, and therefore $C_M/V_R$ was constant, despite a large variability in cell sizes. Assuming a cylindrical cell geometry, the ratio between external surface area to volume is proportional to 2/radius. This means that with increasing cell size the external surface in relation to the volume becomes smaller. Our data indicate, however, that the capacitance-volume relationship was constant over a large range of cell sizes. A cell size dependent increase of the t-tubular fraction of the cell membrane may account for a constant $C_M/V_R$ ratio and may provide a possible explanation for this observation. In an electron micrograph study Page and McCallister (1973) compared the membrane area-to-volume ratio in hypertrophied rat cardiac myocytes and thyroxin-treated animals. They showed that this ratio remained nearly constant and that failure to maintain this ratio may lead to a loss of essential plasma membrane functions and might contribute to the transition from cardiac hypertrophy to heart failure. Furthermore, Keung et al. (1991) provided evidence that the membrane capacitance measured in myocytes from rats with doxorubicin induced cardiomyopathy was lower, consistent with a partial loss of t-tubular membrane and impairment of excitation-contraction coupling due to "detubulation." Isolated ventricular myocytes in culture have been shown to undergo a loss of t-tubules, resulting in significant changes in EC coupling and calcium handling (Lipp et al., 1995). The compensatory change of membrane folding appears to be important for maintaining vital functions of the surface membrane. These functions not only include EC coupling but also uptake of metabolic substrates and extrusion of waste products (Vandewoude and Buyssens, 1992).

## Species and developmental stage dependence of the membrane capacitance-volume relationship

In Fig. 5 we showed that the $C_M/V_R$ ratio, although constant within an individual species, was statistically different among the three species investigated. Furthermore, with increasing age the $C_M/V_R$ ratio increased substantially, presumably because of a developmental stage-dependent extent of membrane folding (see below). In our experiments the capacitance measurements were related to the total cell volume, and no distinction was made between subcellular compartments. With regard to studying ion fluxes across cell membranes and their effect on cytosolic ion concentrations it might be more useful to relate cell membrane capacitance to nonmitochondrial cell volume. Barth et al. (1992) measured the nonmitochondrial cell volume fractions for cardiac myocytes from rabbits (71.1%), ferrets (67.7%), and rats (68.0%). Using these fractions we calculated the nonmitochondrial cell volumes in our experiments and related these values to the cell membrane capacitance measurements. The calculated values were 6.44 ± 0.63 pF/pl in rabbits, 7.96 ± 0.84 pF/pl in ferrets, and 12.42 ± 1.95 pF/pl in rats. When relating to nonmitochondrial cell volume the differences of the *C-V* relationship among different species became more prominent.

In cardiac cells the degree of membrane folding and the fraction of tubular membrane show species dependence and are influenced by developmental factors (Frank et al., 1994). In mammalian ventricular muscle approximately 30–50% (e.g., rat, 33%; rabbit, 41%; Page, 1978) of the total surface membrane area forms the t-tubules, and 20–50% of the tubular membrane fraction is part of the junctional complex with the sarcoplasmic reticulum (Page and Surdyk-Droske, 1979), and there are significant species differences in the surface area-to-cell volume ratio (for a summary see Bers, 1991). The higher $C_M/V_R$ ratio in rats, for example, may be related to the relative importance of SR calcium release (versus calcium influx) during EC coupling and force development in this species (Bers, 1985; Rich et al., 1988).

Nevertheless, interpretations on species- and developmental stage-dependent differences in the *C-V* relationship with regard to mechanisms of EC coupling should be made carefully. First, the sarcolemma also exhibits small pockets or caveolae, which are flask-shaped invaginations that contribute significantly to the surface area of both external and t-tubular sarcolemma. Page (1978) showed that in rabbit papillary muscle, for example, the caveolar plasma membrane contributed 14–21% to the total plasmalemma with no significant difference between t-tubular system and external sarcolemma. Little is known about species dependence and influence of developmental stage on the contribution of caveolae to the total surface membrane. Second, our experimental approach did not allow quantitative determination of the contribution of various membrane fractions to the total surface area. The cell geometry could only be approximated by assuming a cylindrical or spindle shape, and typically showed branches and dents (see the detailed surface features in Fig. 3 *B*). These structural complexities could increase the fraction of the membrane folding. It was our impression that larger cells tend to have more complex geometrical features, particularly in ferrets. Another factor that may affect our volume estimations are possible small changes in cell volume after establishing the whole-cell configuration in our membrane capacitance measurements. Because the filling solution of the electrodes included EGTA, the intracellular perfusion could cause cell relaxation and, as a result, possibly an increase in cell volume. In our experiments there was a noticeable but small increase in $V_R$ (<10%) in rat myocytes, whereas in the other species this phenomenon was not observed.

## Practical implications of the correlation of membrane capacitance and cell volume

In many electrophysiological studies, the membrane capacitance measurements are used to normalize ionic currents to the total surface membrane area and to express the currents in terms of "current densities." In many instances, however,

it would be more desirable to normalize ion currents to the cell volume, because it is the ionic flux per unit cell volume that critically affects various cellular functions such as the contribution of $Ca^{2+}$ influx to the activator calcium for cardiac muscle contraction (Berlin et al., 1994). The 3D reconstruction techniques based on optical sectioning with LSCM proved to be a powerful method for reliable volume measurements and reconstruction of cell surface topography. We further showed that the simple measurements of membrane capacitance can be used as a readily applicable estimate of cell volume because the *C-V* relationship is constant over a large range of cell sizes. The *C-V* relationship, however, is specific for individual animal species and changes during development. We established further evidence that for individual animal species the product of the readily measurable parameters of cell length and width correlates reasonably well with cell volume and may serve as a useful predictor of cell volume.

We gratefully acknowledge the technical assistance of Mrs. Christina Hovance.

Financial support was provided by grants from the National Institute of Health (DMB, LAB), the American Heart Association National Center (LAB), and the Schweppe Foundation Chicago (LAB). LAB is an Established Investigator of the American Heart Association. This work was done during the tenure of an International Research Fellowship of the American Heart Association (LMDD).

## REFERENCES

Barth, E., G. Stämmler, B. Speiser, and J. Schaper. 1992. Ultrastructural quantitation of mitochondria and myofilaments in cardiac muscle from 10 different animal species including man. *J. Mol. Cell Cardiol.* 24: 669–681.

Benitah, J. P., A. M. Gomez, P. Bailly, J. P. D. Ponte, G. Berson, C. Delgado, and P. Lorente. 1993. Heterogeneity of the early outward current in ventricular cells isolated from normal and hypertrophied rat hearts. *J. Physiol.* 469:111–138.

Berlin, J. R., J. W. M. Bassani, and D. M. Bers. 1994. Intrinsic cytosolic calcium buffering properties of single rat cardiac myocytes. *Biophys. J.* 67:1775–1787.

Bers, D. M. 1985. Ca influx and sarcoplasmic reticulum Ca release in cardiac muscle activation during post-rest recovery. *Am. J. Physiol.* 248:H366–H381.

Bers, D. M. 1991. Excitation-Contraction Coupling and Cardiac Contractile Force. Kluwer Academic Publishers, Norwell, MA.

Blatter, L. A., and W. G. Wier. 1992. Agonist-induced $[Ca^{2+}]_i$ waves and $Ca^{2+}$-induced $Ca^{2+}$ release in mammalian vascular smooth muscle cells. *Am. J. Physiol.* 263:H576–H586.

Campbell, S. E., A. M. Gerdes, and T. D. Smith. 1987. Comparison of regional differences in cardiac myocyte dimensions in rats, hamsters, and guinea pigs. *Anat. Rec.* 219:53–59.

Chacon, E., J. M. Reece, A.-L. Nieminen, G. Zahrebelski, B. Herman, and J. J. Lemasters. 1994. Distribution of electrical potential, pH, free $Ca^{2+}$, and volume inside cultured adult rabbit cardiac myocytes during chemical hypoxia: a multiparameter digitized confocal microscopic study. *Biophys. J.* 66:942–952.

Cohen, A. R., B. Roysam, and J. N. Turner. 1994. Automated tracing and volume measurements of neurons from 3-D confocal fluorescence microscopy data. *J. Microsc.* 173:103–114.

Delcarpio, J. B., W. C. Claycomb, and R. L. Moses. 1989. Ultrastructural morphometric analysis of cultured neonatal and adult rat ventricular cardiac muscle cells. *Am. J. Anat.* 186:335–345.

Dodge, D. E., C. G. Plopper, and R. B. Rucker. 1994. Regulation of Clara cell 10 kD protein secretion by pilocarpine: quantitative comparison of nonciliated cells in rat bronchi and bronchioles based on laser scanning confocal microscopy. *Am. J. Respir. Cell Mol. Biol.* 10:259–270.

Drewnowska, K., and C. M. Baumgarten. 1991. Regulation of cellular volume in rabbit ventricular myocytes: bumetanide, chlorothiazide, and ouabain. *Am. J. Physiol.* 260:C122–C131.

Frank, J. S., G. Mottino, F. Chen, V. Peri, P. Holland, and B. S. Tuana. 1994. Subcellular distribution of dystrophin in isolated adult and neonatal cardiac myocytes. *Am. J. Physiol.* 267:C1707–C1716.

Fraticelli, A., R. Josephson, R. Danziger, E. Lakatta, and H. Spurgeon. 1989. Morphological and contractile characteristics of rat cardiac myocytes from maturation to senescence. *Am. J. Physiol.* 257:H259–H265.

Gerdes, A. M., J. A. Moore, J. M. Hines, P. A. Kirkland, and S. P. Bishop. 1986. Regional differences in myocyte size in normal rat heart. *Anat. Rec.* 215:420–426.

Guilak, F. 1994. Volume and surface area measurement of viable chondrocytes in situ using geometric modelling of serial confocal sections. *J. Microsc.* 173:245–256.

Hille, B. 1992. Ionic Channels of Excitable Membranes. Sinauer Associates, Sunderland, MA.

Hryshko, L. V., V. Stiffel, and D. M. Bers. 1989. Rapid cooling contractures as an index of SR Ca content in rabbit ventricular myocytes. *Am. J. Physiol.* 257:H1369–H1377.

Huynh, T. V., F. Chen, G. T. Wetzel, W. F. Friedman, and T. S. Kiltzner. 1992. Developmental changes in membrane $Ca^{2+}$ and $K^+$ currents in fetal, neonatal, and adult rabbit ventricular myocytes. *Circ. Res.* 70: 508–515.

Keung, E. C., L. Toll, M. Ellis, and R. A. Jensen. 1991. L-type cardiac calcium channels in doxorubicin cardiomyopathy in rats morphological, biochemical and functional correlations. *J. Clin. Invest.* 87:2108–2113.

Lipp, P., J. Hüser, L. Pott, and E. Niggli. 1995. Subcellular EC-coupling is controlled by the t-tubules in ventricular myocytes. *Biophys. J.* 68:A417.

Lorensen, W. E., and H. E. Cline. 1987. Marching cubes: a high resolution 3D surface construction algorithm. *Comput. Graphics.* 21:163–169.

Majlof, L, and P.-O. Forsgren. 1993. Confocal microscopy: important consideration for accurate imaging. *Methods Cell Biol.* 38:79–95.

Nash, G. B., P. E. R. Tatham, T. Powell, V. W. Twist, R. D. Speller, and L. T. Loverock. 1979. Size measurements on isolated rat heart cells using Coulter analysis and light scatter flow cytometry. *Biochim. Biophys. Acta.* 587:99–111.

Neher, E., and G. J. Augustine. 1992. Calcium gradients and buffers in bovine chromaffin cells. *J. Physiol.* 450:273–301.

Page, E. 1978. Quantitative ultrastractural analysis in cardiac membrane physiology. *Am. J. Physiol.* 235:C147–C158.

Page, E., J. Earley, and B. Power. 1974. Normal growth of ultrastructures in rat ventricular myocardial cells. *Circ. Res.* 34 and 35(Suppl. II): II-12–II-16.

Page, E., and L. P. McCallister. 1973. Quantitative electron microscopic description of heart muscle cells. Application to normal, hypertrophied and thyroxin-stimulated hearts. *Am. J. Cardiol.* 31:172–181.

Page, E., and M. Surdyk-Droske. 1979. Distribution, surface density, and membrane area of diadic junctional contacts between plasma membrane and terminal cisterns in mammalian ventricle. *Circ. Res.* 45:260–267.

Poole-Wilson, P. A. 1995. The dimensions of human cardiac myocytes; confusion caused by methodology and pathology. *J. Mol. Cell Cardiol.* 27:863–865.

Rich, T. L., G. A. Langer, and M. G. Klassen. 1988. Two components of coupling calcium in single ventricular cell of rabbits and rats. *Am. J. Physiol.* 254:H937–H946.

Rossner, K. L. 1991. Calcium current in congestive heart failure of hamster cardiomyopathy. *Am. J. Physiol.* 260:H1179–H1186.

Scamps, F., E. Mayoux, D. Charlemagne, and G. Vassort. 1990. Calcium current in single cells isolated from normal and hypertrophied rat heart. *Circ. Res.* 67:199–208.

Scheynius, A. M. Dalenbring, K. Carlsson, R. England, and M. Lindberg. 1992. Quantitative analysis of Langerhans' cells in epidermis at irritant contact reactions using confocal laser scanning microscopy. *Acta Derm. Venereol. (Stockh.).* 72:348–351.

Smith, S. H., and S. P. Bishop. 1985. Regional myocyte size in compensated right ventricular hypertrophy in the ferret. *J. Mol. Cell Cardiol.* 17:1005–1011.

Stevens, J. K. 1994. Introduction to confocal three-dimensional volume investigation. *In* Three-Dimensional Confocal Microscopy: Volume Investigation of Biological Systems. Cell Biology. J. K. Stevens, L. R. Mills, and J. E. Trogadis, editors. Academic Press, San Diego. 3–27.

Tinel, H., F. Wehner, and H. Sauer. 1994. Intracellular $Ca^{2+}$ release and $Ca^{2+}$ influx during regulatory volume decrease in IMCD cells. *Am. J. Physiol.* 267:F130–F138.

Tomita, F., A. L. Bassert, R. J. Myerburg, and S. Kimura. 1994. Diminished transient outward currents in rat hypertrophied ventricular myocytes. *Circ. Res.* 75:296–303.

Vandewoude, M. F. J., and N. Buyssens. 1992. Effect of ageing and malnutrition on rat myocardium. I. The myocyte. *Virchows Arch. A Pathol. Anat.* 421:179–188.

Vliegen, H. W., A. van der Laarse, J. A. N. Huysman, E. C. Wijnvoord, M. Mentar, C. J. Cornelisse, and F. Eulderink. 1987. Morphometric quantification of myocyte dimensions validated in normal growing rat hearts and applied to hypertrophic human hearts. *Cardiovasc. Res.* 21:352–357.

Wang, S. Y., L. Winka, and G. A. Langer. 1993. Role of calcium current and sarcoplasmic reticulum calcium release in control of myocardial contraction in rat and rabbit myocytes. *J. Mol. Cell Cardiol.* 25: 1339–1347.

Wettwer, E., G. Amos, J. Gath, H.-R. Zerkowski, J.-C. Reidemeister, and U. Ravens. 1993. Transient outward current in human and rat ventricular myocytes. *Cardiovasc. Res.* 27:1662–1669.

Wright, S. J., V. E. Centonze, S. A. Stricker, P. J, DeVries, S. W. Paddock, and G. Schatten. 1993. An introduction to confocal microscopy and three-dimensional reconstruction. *Methods Cell Biol.* 38:1–45.